International Journal of Mechanical, Industrial and Aerospace Sciences
ISSN: 2517-9950
Vol:6, No:5, 2012

Analytical and Experimental Study on the Effect of Air-Core Coil Parameters on Magnetic Force Used in a Linear Optical Scanner

Loke Kean Koay, Horizon Gitano-Briggs, and Mani Maran Ratnam

Abstract**—** Today air-core coils (ACC) are a viable alternative to ferrite-core coils in a range of applications due to their low induction effect. An analytical study was carried out and the results were used as a guide to understand the relationship between the magnet-coil distance and the resulting attractive magnetic force. Four different ACC models were fabricated for experimental study. The variation in the models included the dimensions, the number of coil turns and the current supply to the coil. Comparison between the analytical and experimental results for all the models shows an average discrepancy of less than 10%. An optimized ACC design was selected for the scanner which can provide maximum magnetic force.

Keywords**—**Air-Core Coils, Electromagnetic, Linear Optical Scanner

I. Introduction

APPLICATIONS of optical scanning are increasing since they are flexible solutions for a variety of technology requirements; some of the applications are in scanners, printers, displays, projectors, bar code scanning, remote measurements of dimensions [1]. Several actuators have been designed to actuate Fast-Steering Mirrors (FSMs). Generally the actuators consist of a galvanometer, piezoelectric actuator, or a voice-coil motor (VCM) [2]. FSMs are defined as optical devices that use a rotatable mirror to reflect light beams between light sources, such as laser beam and a receiver [3]. This study uses a VCM to actuate the FSM in a linear optical scanner since it can provides the desired design characteristics of the scanner such as wide scanning angle and targeted oscillation frequency as shown in a previous study [4].

The structure of VCM can be understood by observing the components used in a traditional electrodynamics speaker. It consists of a coil and a permanent magnet that is joined with the compliant structure of FSM. The presence of iron core in VCM's coil leads to several kinds of nonlinearities. These include the Eddy currents, the magnetic saturation of iron and the variation of coil inductance with its position thus causing reluctance force effect [5]. These drawbacks can be overcome by using ACCs which have no hysteresis caused by ferromagnetic materials, no eddy current losses, and no flux saturation [6]. However the electromagnetic behaviors of the ACC are affected by various parameters such as the coil dimensions and number of coil turns.

L.K. Koay. Author is with the School of Mechanical Engineering, Engineering Campus, Universiti Sains Malaysia, 14300, Nibong Tebal, Penang, Malaysia. (phone: +6016-4340182; e-mail: lkean85@hotmail.com).

H. Gitano-Briggs. Author, Prof., is with the School of Mechanical Engineering, Engineering Campus, Universiti Sains Malaysia, 14300, Nibong Tebal, Penang, Malaysia. (phone: +6016-4846524; e-mail: horizonusm@yahoo.com).

M. M. Ratnam. Author, Prof., is with the School of Mechanical Engineering, Engineering Campus, Universiti Sains Malaysia, 14300, Nibong Tebal, Penang, Malaysia. (phone: +604-5996325; e-mail: mmaran@eng.usm.my).

One of the goals for the linear optical scanner research currently being pursued by researcher is to create scanners that are able to provide a wide scanning angle. Various methods have been investigated to achieve this goal [4]. One of the methods used in this study is by actuating the FSM with higher magnetic forces to attain wide scanning angle.

The existing ACC is unable to provide the required displacement angle. Thus the present study was undertaken to optimize the ACC design and achieve the goal of wide scanning angle. Four different ACCs were studied for the experimental-analytical results validation. Then an optimized ACC which is able to provide maximum magnetic force and thus a large displacement angle was selected. Investigating the performance of such systems early in the design process can significantly impact the cost and improve the design quality.

A. Linear Optical Scanner

The linear optical scanner designed for this study consists of mounting the mirror and suspended plate on a mechanically-resonant torsional spring as shown in Fig. 1. Electric current supplied through the coil induced the magnetic field which interacts with the magnet and causing angular deflection of the mirror. The size of the components (suspended plate, torsional spring, and mirror) as shown in Fig. 1 are 85 mm × 50 mm × 10 mm ($L \times W \times T$). The weight of those components (suspended plate, torsional spring, and mirror) are about 6.50 g.

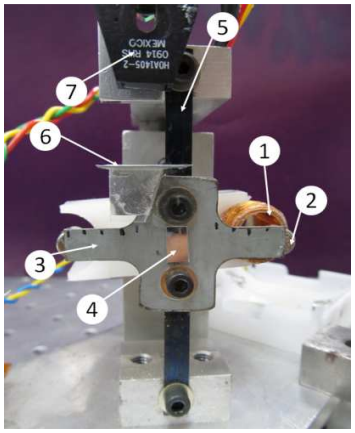

Fig. 1 Torsional spring scanner: (1) Air-Core Coil (2) Magnet (3) Suspended Plate (4) Mirror (5) Torsional Spring (6) Sensor Target (7) Photodiode Sensor

B. Air-Core Coil

A 0.3454 mm diameter copper wire (SWG 29) was used in winding the ACCs in this study to avoid coil overheating due to larger coil diameter. Additionally it can produce the required magnetic flux. When overheating occurs it deteriorates the magnetic flux and hence the magnetic force produced by the coil.

The experimental setup shown in Fig. 2 was used to control the bipolar ACC. The bipolar ACC has a single winding per phase, thus the magnetic force produced is either attractive or repulsive. A controller is required to power the two phases using a H-bridge in this scanner [7]. The H-bridge consists of n-p-n and p-n-p transistors which function as swiches to power the bipolar coils. By repeatedly switching the current supply direction, the attractive-repulsive forces acting on the magnet will induce oscillation of the mirror. Then, a laser reflected from the mirror and creates a linear scanned beam on a screen. A feedback control system is used to synchronize the phases of magnetic force to the angular displacement of FSM. Therefore, a maximum angular displacement can be obtained by actuating at system's resonant frequency. Measurement of the angular displacement of FSM was performed using the signal from a photodiode sensor connected to a Data Acquisition System (DAQ) as shown in Fig. 2.

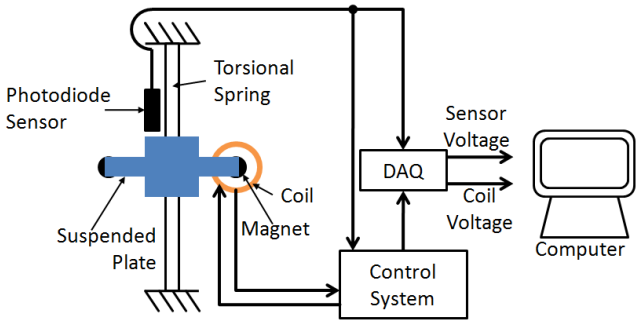

Fig. 2 Experimental setup used in the study

C. Neodymium Magnet

A cylindrical neodymium magnet of 8mm length and 6 mm diameter was selected for the study since it is able to provide the required magnetic force.

D. Suspended Plate Design

The desired angular displacement of the scanner is 30°. Therefore, an "angular displacement envelop" of 30° is needed for the oscillation path. The original design of the suspended plate consists of an in-plane t-shape galvanized iron as shown in Fig. 3(a). There are some disadvantages of using this design as it causes mechanical interference with ACC as shown in Fig. 4. To attain angular displacement envelop, modification of the suspended plate was performed as shown in Fig. 3(b). To maintain the location of the magnet at 21.5 mm from the twist axis as shown in Fig. 4, the suspended plate was lengthened to allow a 45° bend at 8 mm from twist axis. By the 45° bending, the magnet can now move into the core space of the coil without causing mechanical interference.

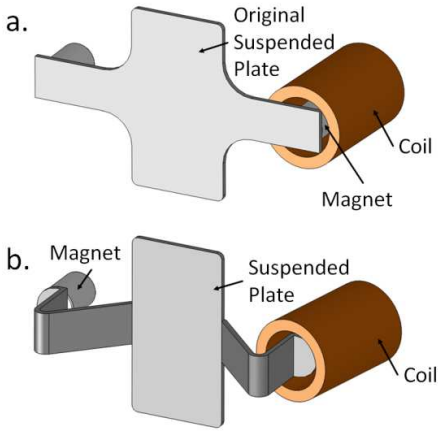

Fig. 3 Suspended plate designs: (a) Original design (b) Modified design

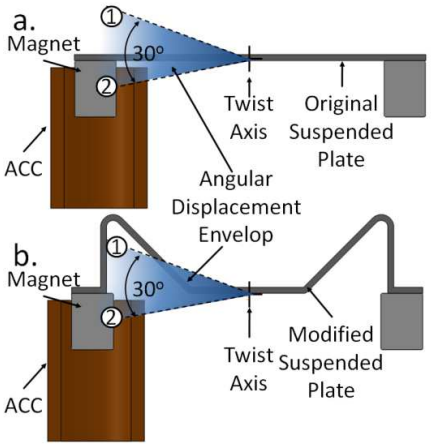

Fig. 4 Plan view of the suspended plate designs: (a) Original design (b) Modified design

II. Theoretical Formulation of Magnetic Force

A. Force Characteristic of Magnetic Force

To determine the magnetic force between the ACC and permanent magnet, a z-direction magnetic dipole moment was assumed as shown in Fig. 5.

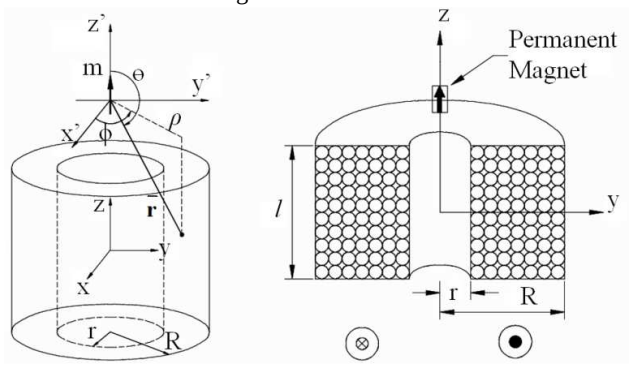

Fig. 5 Air-core coil [6]

The equation of the magnetic force F relative to a permanent magnet in the z-direction can be expressed in terms of the

external magnetic field density/ magnetic flux density *B* and its gradient as [8],

$$F = (m_z.\nabla)B \quad \text{or} \quad F_n = m_z \frac{\partial B_n}{\partial z} \tag{1}$$

where

$m_z$is the magnetic dipole moment

n is x,y,z-direction

The magnetic dipole moment is calculated by $I \times S$, where S is the surface area of the loop and I is the current of the loop. The magnetic forces can be calculated based in the quantification of the magnetic field density. The magnetic field density produced by the steady current density in a closed circuit can be represented by the Biot-Savart law. According to the law, the magnetic field density, B at an arbitrary point z can be calculated by [8],

$$B_z = \frac{\mu_0 I a^2}{4\pi(a^2+z^2)^{3/2}} \int_0^{2\pi} d\phi = \frac{\mu_0 I a^2}{2(a^2+z^2)^{3/2}} \tag{2}$$

where

μ_0 is the permeability of the empty space

a is the radius of the loop

Since the current is supplied into a multi layer ACC proposed for this study, the structure considered is a superposition of a sequence of circular current loops in the axial direction and in the radial direction as shown in Fig. 5. An approximation solution for a multi layer ACC was proposed by Jung et al. [6]. By integrating (2) in radial and longitudinal directions, calculating the means value, then multiplying with the number of turns on the ACC; the resultant magnetic field density can be determined as shown in (3). This approximation is acceptable when the number of turns is large, after integration performed [6],

$$B_z = \frac{\mu_0 NI}{2l(R-r)} \left[\left(z+\frac{l}{2}\right) \ln \frac{R+\sqrt{R^2+(z+l/2)^2}}{r+\sqrt{r^2+(z+l/2)^2}} + \left(z-\frac{l}{2}\right) \ln \frac{r+\sqrt{r^2+(z-l/2)^2}}{R+\sqrt{R^2+(z-l/2)^2}} \right] \tag{3}$$

where

N is coil turns

l, R, *and* r are dimensions shown in Fig. 5

The magnetic force that acts on a point in the z-direction can be obtained by substituting (3) into (1). A derived magnetic force in z-axis function is shown in the Appendix.

After the study on the calculation of magnetic force, the analytical equation is substituted with the parameters which are presented in next section to obtain the analytical data. However, this magnetic force approximation is limited to points located along the axis and thus validation from experimental results is required to make sure the predicted trends are correct. Another simplification in the study is linear magnet travel path was used for experimental study. In the actual case, a curve magnet travel path as shown in Fig. 6 was found, where the magnet is nonparallel with the ACC when oscillation.

III. Methodology

A. Air-Core Coil Constraint

Initial dimensions of the ACC were designed under the constraints of the product envelop as shown in Fig. 6. Due to the product envelop constraint and to avoid the mechanical interference between the ACC and the magnet located at the end of suspended plate, the ACC's outer radius R was set to be less than 9 mm while the inner radius r is set to be more than 5 mm. Similarly, the length of ACC was set to be less than 23 mm due to product envelop constraint. The dimensional constraints of the ACC are shown in Table 1.

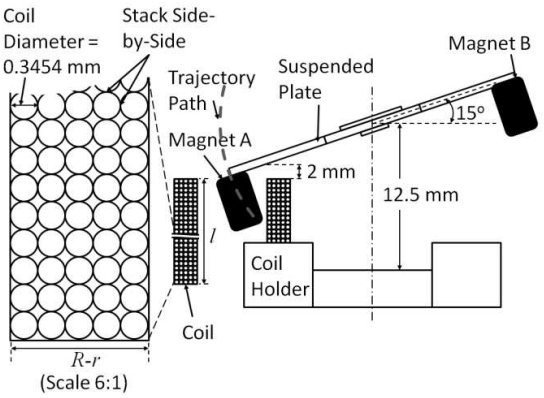

Fig. 6 Product envelope (Plan View)

TABLE I
Dimensions Constraint of Acc (mm)

Length, l	≤23.0
Inner radius, r	≥5.0
Outer radius, R	≤9

Another factor that influences the magnetic forces of an ACC is the current supply. Therefore, two different values of direct current (0.5 A and 1 A) were supplied to the ACC and a comparison for the induced magnetic forces was obtained.

B. Air-Core Coil Design

Four models were designed for geometry study by varying the length, inner radius, and outer radius subjected to the following constraints. Two dimensions of the ACC (length, inner radius, and outer radius) were held constant while another dimension was allowed to vary from model to model. The specifications of ACC models were organized in Table 2. Model 1 is the original ACC used in the linear optical scanner. As observed in Table 2, for Model 1 to 2 the inner radius and length is held to be about the same while the outer radius is changed from 6.9 mm to 7.7 mm. The inner radius and the outer radius were held roughly constant while the length was allowed to change from Model 2 to 3. Lastly, the inner radius and length were held to be about the same while the outer radius was allowed to change from Model 3 to 4. In this study, the ACCs were wound around a removable bobbin. The bobbin was withdrawn after the desired dimensions of ACC were achieved. Then, the winding are secured with Cyanoacrylate hardening agent. As observed in Table 2, a deviation of about 0.45% for r

from 5.275 (Model 1) to 5.250 (Model 2) was found. However the deviation deemed to be acceptably small for this geometry study since it is merely used as a guide to improve the ACCs design.

TABLE II
SPECIFICATION OF COIL MODEL

	Model 1	Model 2	Model 3	Model 4
Inner radius, r (mm)	5.275	5.250	5.225	5.000
Outer radius, R (mm)	6.900	7.690	7.913	8.880
Length, l (mm)	21.50	22.20	11.90	11.80
Number of turns, N	200	320	250	330
Current density, J (MA · m^{-2})	2.86	2.95	3.91	3.60

In Table II, direct current of 0.5 A is used in the calculation for current density. The current density was determined with (4).

$$J = \frac{NI}{(R-r)l} \tag{4}$$

According to the coil geometry calculation by assuming wire stacked side-by-side as shown in scaled up (6:1) window in Fig. 6, the number of turns for Model 1 should be 292 turns and Model 3 should be less (268 turns). However, as observed in Table 2 the number of turns for Model 1 (200 turns) is less than Model 2 (320 turns) due to the stacking inconsistency when winding process. The stacking inconsistencies cause variation in current density. A minor stacking inconsistency is considered to be secondary effect as long as the required dimensional constraints and the number of coil turns are achieved.

C. Experimental Setup

To investigate the magnetic force act on the magnet, a Lutron (TQ-8800) torque meter was used as shown in Fig. 7. The high resolution mode of 0.1 Ncm was selected for the measurement of the torque induced from the ACC. An "L" bar (Fig. 8) was mounted in the torque meter's chuck in order to create a torque arm for the magnet which is attached at the end of the bar. With the "L" bar, the calculation for magnetic force of the ACC can be performed by dividing the torque reading to the torque arm length (80 mm). To examine the magnetic forces between the ACC and the magnet with the variation of magnet-coil distance, a micrometer is used to hold the ACC. The function for using the micrometer is to increase data collection accuracy since small distance increment was achievable. The data points were collected with the increment of 0.5mm from the distance of magnet to the ACC. The results are given in the graphical form as shown in next section.

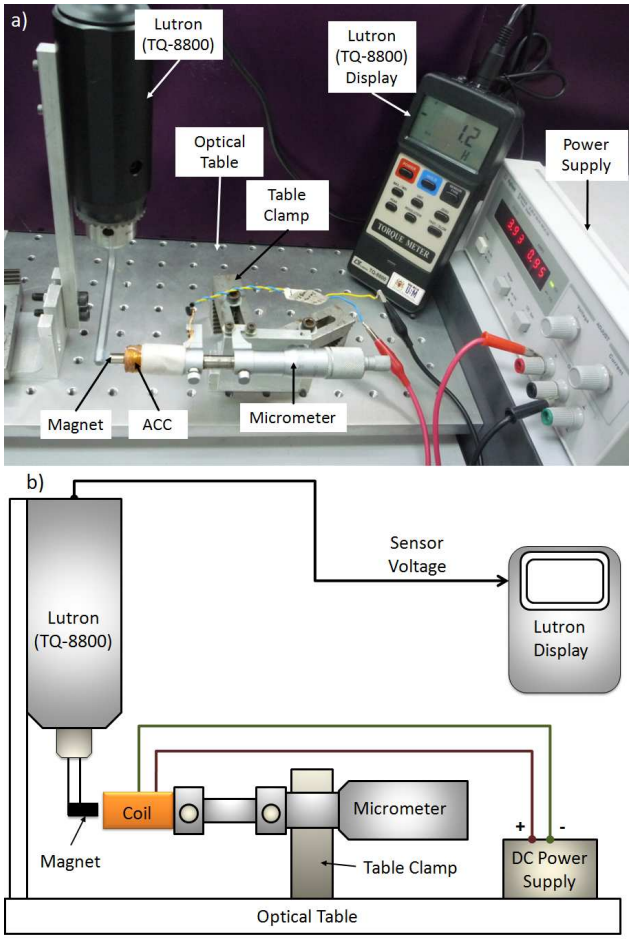

Fig. 7 Experimental setup to measure magnetic force: (a) Photograph of the setup (b) Schematic diagram of the setup

IV. RESULTS AND DISCUSSION

A. Validation of Analytical Results with Experimental Results

Fig. 9 shows the analytical and experimental magnetic force obtained for ACC Model 1 as a function to the magnet-coil separation. As observed, the distance of ACC from magnet can be separated into two regions; they are negative region at the left hand side and positive region at right hand side. This is due to the definition of zero point for the distance of ACC from magnet as shown in Fig. 10, where the penetrating of magnet to the left hand side of ACC was defined to be in negative region and vice versa. Average discrepancies of 1.6% and -8.05% are found in the comparison of the analytical magnetic forces and experimental magnetic forces for the current supply of 0.5 A and 1 A respectively. Therefore the data collected experimentally and analytically are valid for the study since it merely acts as a guide for the selection of optimized ACC model. As observed in Fig. 9, the magnetic forces obtained from ACC with current 1 A is approximately twice the forces obtained from ACC with current 0.5 A. This is due to the doubling of current density for similar ACC model.

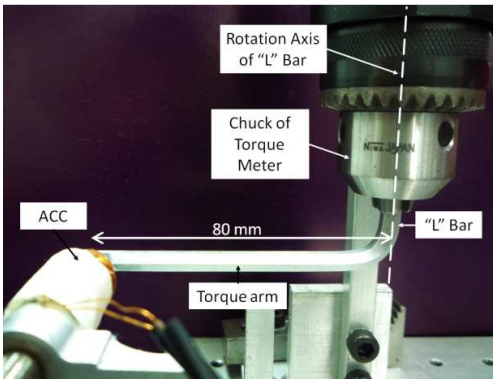

Fig. 8 Torque arm of the "L" bar

Another interesting result in the study is the maximum magnetic force was found to be occurred at about the halfway of the magnet's length (4 mm) when the ACC was travelled along the magnet. Thus, the maximum magnetic force (0.20 N for I=1 A and 0.10 N for I=0.5A) of the ACC occurred at the negative region of the ACC (-5 mm) as shown in Fig. 10. This also indicates that ACC can use the advantages of small product envelop for the product design while maintaining the amount of power or force provided to the system since the magnet-coil distance is shorter.

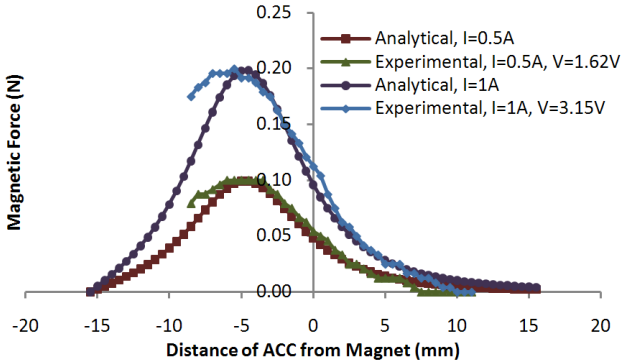

Fig. 9 Magnetic force between coil and magnet versus distance from magnet for Model 1

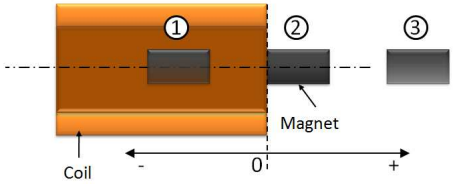

Fig. 10 Cross-sectioned of ACC, position 2 is zero of distance from magnet to ACC, position 1 is negative region and position 3 is positive region

Fig. 11 shows the magnetic force created between the ACC Model 2 and magnet to the distance of ACC from magnet. Average discrepancies of -8.74% and -6.30% are found in the comparison of the analytical magnetic forces and experimental magnetic forces for the current supplies of 0.5 A and 1 A respectively. The maximum magnetic force also occurs when about half of the magnet penetrates the ACC with 0.25 N for current 1 A and 0.125 N for current 0.5 A respectively.

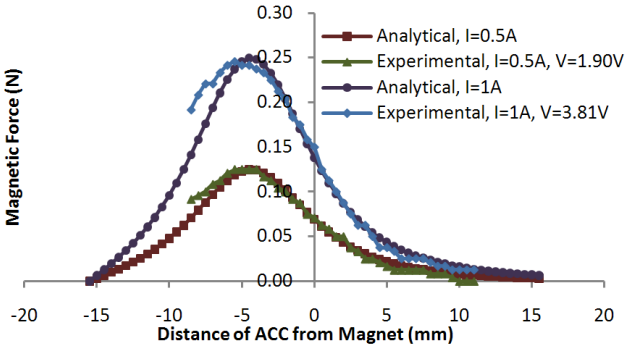

Fig. 11 Magnetic force between coil and magnet versus distance from magnet for Model 2

Similarly, average discrepancies of -9.80% and -9.63% are found in the comparison of the analytical magnetic forces and experimental magnetic forces for the current supplies of 0.5 A and 1 A as shown in Fig. 12 for ACC Model 3. The length (about 10 mm) of the ACC in Model 3 and 4 is about half of the length (20 mm) of ACC in Models 1 and 2. However, once again, the maximum magnetic force occurs at about 50% magnet penetration with 0.37 N for 1 A and 0.22 N for 0.5 A with Model 3. These results showed that the location of the peak magnetic force arise mainly depend on the length of magnet but not on the length of ACC.

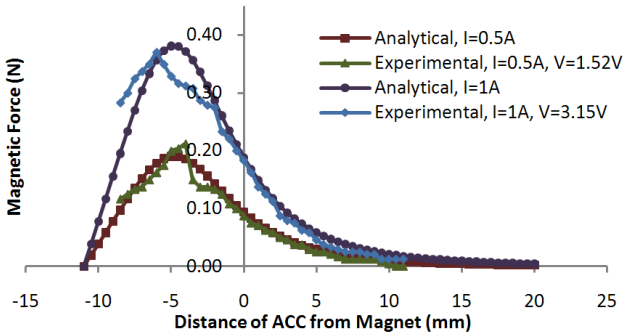

Fig. 12 Magnetic force between coil and magnet versus distance from magnet for Model 3

ACC Model 4 gave the average discrepancies of -9.30% and -9.53% on the comparison of the analytical results and experimental result for the current supplies of 0.5 A and 1 A respectively as shown in Fig. 13.

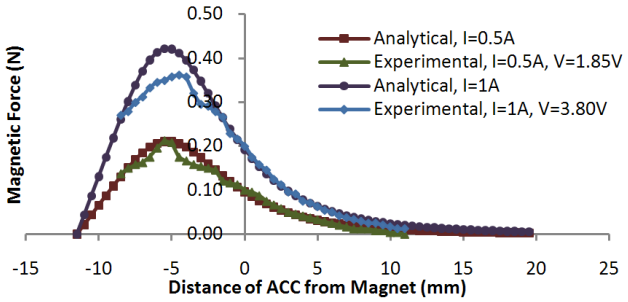

Fig. 13 Magnetic force between coil and magnet versus distance from magnet for Model 4

A comparison of the maximum magnetic force among the models is shown in Table III after the validation of the aforementioned results.

TABLE III
COMPARISON OF THE MAGNETIC FORCE FOR VARIOUS MODELS

	Model 1	Model 2	Model 3	Model 4
Maximum Magnetic Force, Current, I=1 A	0.20 N	0.25 N	0.37 N	0.35 N
Maximum Magnetic Force, Current, I=0.5 A	0.10 N	0.125 N	0.22 N	0.20 N
Current density, J (MA $\cdot$ m^{-2})	5.72	5.91	7.82	7.21

The current density determined on the ACC models as shown in Table 3 are calculated by substituting direct current of 1 A into (4). According to the experimental results, Model 3 yields the maximum magnetic force of 0.37 N (1 A) and 0.22 N (0.5 A) at about -5.5 mm from the tip of the ACC due to the highest current density of the ACC (7.82 MA $\cdot$ m^{-2}). Thus, ACC Model 3 is selected to be the optimized ACC design due to the maximum magnetic force. It give us an 85 % improvement in the magnetic force compared to the original ACC Model 1 (0.2 N at I=1 A). Based on this we believe that the optimum ACC Model 3 will have maximum scanning angle in excess of the required criteria of the scanner operation.

V. CONCLUSIONS

The magnetic force of the air-core coil and neodymium magnet in a scanner was investigated using analytical and experimental methods to obtain the optimized model. Several ACC designs were then selected for study subjected to certain dimensional constraints. The dimensional constraints included the length, the inner radius, and the outer radius of ACC. Four ACCs were fabricated for the experimental analysis. Results of the numerical calculation agreed with the measured values of magnetic force to within average discrepancy of 10%. Magnetic force of ACC Model 3 indicated 85% higher than the previously developed design. According to the results obtained, the peak magnetic forces were located at about 50% of magnet penetration. Therefore, ACCs have the advantage of utilizing the smaller product envelope while maintaining scanning angle of the scanner.

Since the coils were tested in static mode without operating at resonant frequency, another study will be carried out in dynamic mode at resonant frequency as the future work. We believe it will provide an interesting study for the energy consumption characteristic of the ACCs.

APPENDIX

$$F_z = \frac{\mu_0 mN}{2(R-r)l}\left\{\ln\left[\frac{R+\frac{1}{2}\sqrt{4R^2+4z^2+4zl+l^2}}{r+\frac{1}{2}\sqrt{4r^2+4z^2+4zl+l^2}}\right]+\frac{1}{R+\frac{1}{2}\sqrt{4R^2+4z^2+4zl+l^2}}\left[\left(z+\frac{1}{2}l\right)\left(\frac{\frac{1}{4}\frac{8z+4l}{\sqrt{4R^2+4z^2+4zl+l^2}\left(r+\frac{1}{2}\sqrt{4r^2+4z^2+4zl+l^2}\right)}-\frac{\left(R+\frac{1}{2}\sqrt{4R^2+4z^2+4zl+l^2}\right)(8z+4l)}{\frac{1}{4}\left(r+\frac{1}{2}\sqrt{4r^2+4z^2+4zl+l^2}\right)^2\sqrt{4R^2+4z^2+4zl+l^2}}\right)\right]+\left(r+\frac{1}{2}\sqrt{4r^2+4z^2+4zl+l^2}\right)\right]+\ln\left[\frac{r+\frac{1}{2}\sqrt{4r^2+4z^2-4zl+l^2}}{R+\frac{1}{2}\sqrt{4R^2+4z^2-4zl+l^2}}\right]+\frac{1}{r+\frac{1}{2}\sqrt{4r^2+4z^2-4zl+l^2}}\left[\left(z-\frac{1}{2}l\right)\left(\frac{\frac{1}{4}\frac{8z-4l}{\sqrt{4r^2+4z^2+4zl+l^2}\left(R+\frac{1}{2}\sqrt{4R^2+4z^2-4zl+l^2}\right)}-\frac{\left(r+\frac{1}{2}\sqrt{4r^2+4z^2-4zl+l^2}\right)(8z-4l)}{\frac{1}{4}\left(R+\frac{1}{2}\sqrt{4R^2+4z^2-4zl+l^2}\right)^2\sqrt{4R^2+4z^2-4zl+l^2}}\right)\right]+\left(R+\frac{1}{2}\sqrt{4R^2+4z^2-4zl+l^2}\right)\right]\right\}$$

ACKNOWLEDGMENT

The work was financially supported by The Vice-Chancellor's Award of Universiti Sains Malaysia.

REFERENCES

[1] Asada N., Takeuchi M., Vaganov V., and Belov N., 2000, "Silicon micro-optical scanner," Sensors and Actuators A: Physical, **83**(1-3), pp. 284–290.

[2] Xiang S., Chen S., Wu X., Xiao D., and Zheng X., 2010, "Study on Fast Linear Scanning for a New Laser Scanner," Opt. Laser Technol., **42**(1), pp. 42-46.

[3] Zhou J., Yin H., and Wang Y., 2009, "Research on the Structure and Dynamic Characteristics of a Fast-Steering Mirror," Proc. SPIE, **7281**, p. 72810J-72810J-5.

[4] Koay L. K., and Gitano-Briggs H., 2011, "Design and Optimization of Mechanically Resonant Torsional Spring Mechanism for Laser Light Dispersion Applications," ASME J Mech. Des., **133**(1), p. 014504.

[5] Remy M., Lemarquand G., Castagnede B., Guyader G., and Renault T., 2008, "Ironless and Leakage Free Voice-Coil Motor Made of Bonded Magnets," Most, **44**(11), pp. 4289-4292.

[6] Jung K. S., 2002, "Development of a novel maglev positioner with self-stabilizing property," Mechanical Engineering, **12**, pp. 771-790.

[7] Al W., 2002, Microcontroller Project Using the Basic Stamp, Focal Press.

[8] Wangness R. K., 1979, Electromagnetic Fields, John Wiley & Sons, New York.